PHYSICAL REVIEW B **71**, 115213 (2005)

Microvoid formation in hydrogen-implanted ZnO probed by a slow positron beam

Z. Q. Chen,* A. Kawasuso, Y. Xu, and H. Naramoto
Advanced Science Research Center, Japan Atomic Energy Research Institute, 1233 Watanuki, Takasaki, Gunma 370-1292, Japan

X. L. Yuan and T. Sekiguchi
Nanomaterials Laboratory, National Institute for Materials Science, 1-2-1 Sengen, Tsukuba, Ibaraki 305-0047, Japan

R. Suzuki and T. Ohdaira
National Institute of Advanced Industrial Science and Technology, 1-1-1 Umezono, Tsukuba, Ibaraki 305-8568, Japan
(Received 12 November 2004; revised manuscript received 24 January 2005; published 29 March 2005)

ZnO crystals were implanted with 20–80 keV hydrogen ions up to a total dose of 4.4×10^{15} cm^{-2}. Positron lifetime and Doppler broadening of annihilation radiation measurements show introduction of zinc vacancy-related defects after implantation. These vacancies are found to be filled with hydrogen atoms. After isochronal annealing at 200–500 °C, the vacancies agglomerate into hydrogen bubbles. Further annealing at 600–700 °C causes release of hydrogen out of the bubbles, leaving a large amount of microvoids. These microvoids are annealed out at high temperature of 1000 °C. Raman spectroscopy for the implanted sample shows the enhancement of vibration modes at about 575 cm^{-1}, which indicates introduction of oxygen vacancies. These oxygen vacancies disappear at temperatures of 600–700 °C, which is supposed to contribute to the hydrogen bubble formation. Cathodoluminescence measurements reveal that hydrogen ions also passivate deep level emission centers before their release from the sample, leading to the improvement of the UV emission.

DOI: 10.1103/PhysRevB.71.115213 PACS number(s): 61.80.Jh, 78.70.Bj, 61.72.Ji

I. INTRODUCTION

Due to the wide band gap (3.4 keV) and large exciton binding energy (60 meV), zinc oxide (ZnO) has been recognized as a promising candidate for the production of short-wavelength optoelectronic devices, such as UV light-emitting diodes and lasers.[1,2] Recently, the behavior of hydrogen in ZnO has attracted much attention,[3–16] because it may not only enhance the *n*-type conductivity suggested by both theoretical prediction[3] and experimental measurements,[4,5] but may also improve the optical properties by increasing the UV emission efficiency.[7–10] The hydrogen impurities are incorporated unintentionally during the crystal growth with concentration on the order of 10^{16} cm^{-3},[5,6] and are proposed to be the reason for the intrinsic *n*-type conductivity in ZnO.[3] They can also be introduced with high concentration through plasma treatment,[7–12] annealing in H_2 ambient,[13] and ion-implantation technique.[4,14–16] However, up to now most of these studies have been concerned primarily with the electrical and optical properties of ZnO. There is still a lack of fundamental study of the interaction between hydrogen and intrinsic defects, which would help us to obtain a deeper understanding of the role played by hydrogen with respect to the electrical conduction and luminescence properties.

To study the possible interaction between hydrogen and defects, we incorporated hydrogen into ZnO using an ion-implantation technique, which would also produce a large number of defects. The introduction and thermal evolution of the defects were studied by positron annihilation measurements. Positron annihilation spectroscopy is a unique tool to study vacancy defects in semiconductors.[17] The positron is particularly sensitive to vacancy-type defects, in which the positron annihilation characteristics are quite different from the defect-free bulk state. Some preliminary studies have been conducted on the identification of as-grown as well as irradiation-induced defects in ZnO by using this method.[18–23] In this paper, Raman-scattering measurements were also conducted for a complementary study of the defects. The effect of hydrogen on the luminescence properties before and after annealing was characterized by cathodoluminescence measurements. Our results show that hydrogen has a strong interaction with the implantation-induced vacancy defects, and these vacancies evolve into hydrogen bubbles and microvoids during the annealing process.

II. EXPERIMENT

Hydrothermally grown ZnO single crystals were purchased from the Scientific Production Company (SPC Goodwill), which are undoped with an *n*-type conductivity. Hydrogen implantation was performed at room temperature with multiple energies ranging from 20 to 80 keV using a 400 keV implanter. By choosing appropriate doses for each energy, a box-shaped implantation profile can be formed. Detailed implantation parameters are listed in Table I. The beam flux is about 1.2×10^{12} cm^{-2} s^{-1}, and the total dose amounts to about 4.4×10^{15} cm^{-2}. The implanted samples were annealed isochronally in a nitrogen ambient from 200 to 1100 °C for 30 min.

Doppler broadening of positron annihilation spectra were measured using a slow positron beam (0.2–30 keV). Positron lifetime spectra were also measured using a pulsed slow positron beam in National Institute of Advanced Industrial Science and Technology of Japan.[24] The conventional *S* parameter, which is defined as the ratio of the central region

 ©2005 The American Physical Society

TABLE I. Detailed information about the ion implantation. The ion range is obtained from TRIM[26] simulation.

Energy (keV)	Dose (10^{15} cm^{-2})	Range (nm)
20	0.8	204
30	0.45	275
40	0.65	343
50	0.45	406
60	0.50	467
70	0.50	528
80	1.0	585

(511 ± 0.77 keV) to the total area of the 511 keV annihilation peak, is used to analyze the measured Doppler broadening spectra. In this paper, the *S* parameters are normalized to the value in the bulk region of the as-grown sample. Therefore, an increase of the *S* parameter to larger than unity indicates introduction of vacancy defects.

Micro-Raman-scattering measurements were performed using the NANOFINDER spectrometer in the wave number range of 200–800 cm^{-1} with a spectral resolution of <4 cm^{-1}. The 488.0 nm line of a nonpolarized Ar^{+}-ion laser was used for excitation and the incident laser power was ~ 1 mW. The scattered light was detected in the backscattering geometry. The measurement time was 60 s for each spectrum. Cathodoluminescence (CL) spectra were measured using a modified scanning electron microscope (TOPCON DS-130). A monochromator with grating of 100 lines/mm (Jobin Yvon HR320) and a CCD were used for the detection of spectra.[25] The electron-beam energy and current for excitation were 5 keV and 1 nA, respectively, and the acquisition time for each measurement was 5 s. In order to assure the same condition in the Raman and CL measurements after each annealing step, we repeatedly measured one reference sample, and found little change. This indicates that the measurement is highly repeatable. All the above measurements were performed at room temperature.

III. RESULTS AND DISCUSSION

A. Positron annihilation measurements

Figure 1 shows the *S* parameter as a function of incident positron energy (*S-E* curve) for the as-grown and H^{+}-implanted ZnO. For the as-grown sample, the *S* parameter decreases gradually from the surface state to the bulk state with increasing energy, and becomes constant at $E > 7$ keV. After H^{+} implantation, we can see an increase of the *S* parameter in the energy range of 5–15 keV. This means that H^{+} implantation produces vacancy defects in ZnO. However, the *S* parameter (1.01–1.02) is significantly smaller than the reported value of 1.039 for zinc monovacancies.[22]

To decide the size of these vacancies, we measured the positron lifetime for the H^{+}-implanted sample. The lifetime spectra are shown in Fig. 2, and the analyzed lifetime results are listed in Table II. For the as-grown sample, there is only

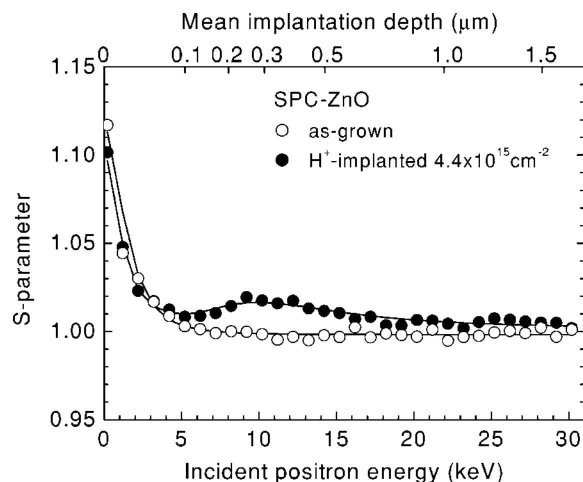

FIG. 1. *S* parameter as a function of incident positron energy measured for ZnO samples before and after H^{+} implantation. The lines are drawn to guide the eye.

one lifetime component, which is about 182 ± 1 ps. This is in good agreement with our previous value of the positron bulk lifetime in ZnO,[21] indicating no positron trapping by vacancies, or that the vacancy concentration is very low. After H^{+} implantation, there is still only one lifetime, but it increases to about 202 ± 1 ps. For the monovacancies in ZnO, only zinc vacancy (V_{Zn}) can be observed by positrons.[19,21,22] However, the experimental positron lifetime for V_{Zn} is around 230 ps.[22] This is apparently longer than the positron lifetime measured in our H^{+}-implanted sample.

One possible reason for the small increase of the positron lifetime and *S* parameter is that the H^{+} implantation-induced vacancy concentration is not high enough to cause saturated trapping of positrons. Therefore, the measured positron lifetime and *S* parameter are just averages of the free and trapped states. To elucidate this possibility, we also listed in Table II our positron lifetime result for the electron-irradiated ZnO at some selected doses for a comparison. From the TRIM simulation,[26] the hydrogen implantation produces a total vacancy concentration as high as $8-9 \times 10^{20}$ cm^{-3}, while the calculated vacancy concentration produced by 3-MeV elec-

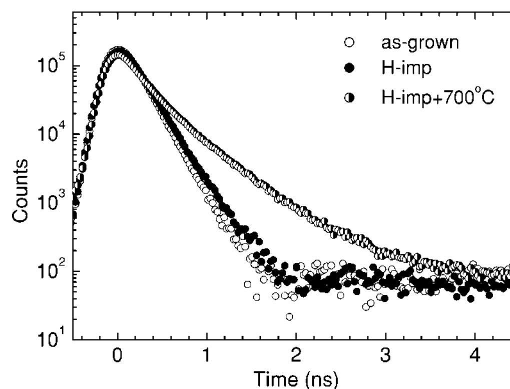

FIG. 2. Positron lifetime spectra measured for ZnO samples before and after H^{+} implantation and 700 °C annealing. The incident positron energy is 10 keV for the as-grown sample, and 7 keV for the implanted samples.

TABLE II. Positron lifetime results for the ZnO sample before and after H^+ implantation and annealing. The positron lifetime data in the 3 MeV electron-irradiated ZnO at some selected doses are also listed for a comparison.

Sample	τ_1 (ps)	I_1 (%)	τ_2 (ps)	I_2 (%)	τ_{av} (ps)
As-grown	182.2±0.7	100	–	–	182.2
H^+-implanted	202.0±0.6	100	–	–	202.2
H^+-impl.+700 °C	173.2±6.0	48.0±2.0	416.1±9.2	52.0±2.0	299.5
1×10^{18} e^-/cm^2	161.8±14	44±22	216.0±11	56±22	192.4
5.5×10^{18} e^-/cm^2	151.7±14	22.7±8.0	230.8±4.4	77.3±8.0	212.3

trons with a maximum dose of 5.5×10^{18} cm^{-2} is only about 2×10^{19} cm^{-3}. However, we observed an average positron lifetime of 212 ps in the 5.5×10^{18} cm^{-2} electron-irradiated sample, which is higher than that of the H^+-implanted sample. This comparison indicates that the short positron lifetime in the H^+-implanted sample is not due to low vacancy concentration. It is known that hydrogen is a very active impurity, which will passivate intrinsic defects in many metals and semiconductors.[27] In ZnO, formation of O–H bonds inside V_{Zn} has been proposed.[11] Due to the filling of hydrogen impurities in the vacancies, the positron lifetime or S parameter will decrease considerably. Similar behavior has been observed by many authors.[28–31] Therefore, the vacancies produced by H^+ implantation are most probably filled with hydrogen atoms, and these vacancies are supposed to be V_{Zn}. However, we cannot exclude the possibility of divacancies that are filled with more hydrogen impurities; thus, the positron has a similar lifetime in them. The hydrogen has less chance to fill in the oxygen vacancy (V_O), because the Zn–H bond is much weaker than the O–H bond.[11] However, because the positron is not sensitive to V_O, we cannot prove it using this method.

Figure 3 shows some selected S-E curves as a function of annealing temperature for the H^+-implanted ZnO. At lower temperatures, S-E curve has nearly no change. However, after annealing at above 500 °C, the S parameters in the implanted region (5–15 keV) begin to increase. At 700 °C, the S parameters increase abruptly, after which they begin to decrease, and finally attain the bulk value at 1100 °C.

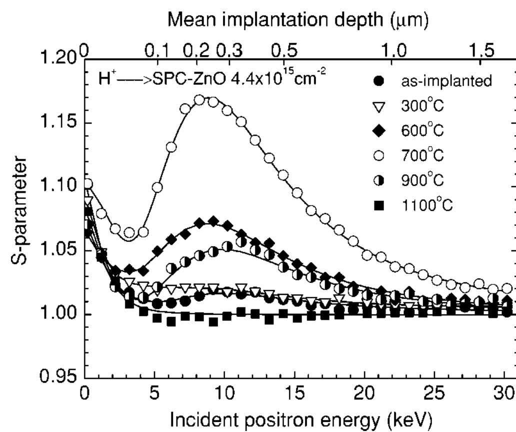

FIG. 3. Annealing behavior of the S-E curves measured for the H^+-implanted ZnO. The lines are drawn to guide the eye.

We summed together the Doppler broadening spectra measured in the incident positron energy range of 7–10 keV, which corresponds to the central implanted region, and calculated the average S parameter as a function of annealing temperature, which is shown in Fig. 4. Three annealing periods can be seen clearly from this figure. In the first period (0–500 °C), the S parameter shows a slight increase with increasing temperature. In this process, agglomeration of vacancy clusters is expected to take place. The hydrogen-decorated V_{Zn} might not be able to migrate. However, they can absorb mobile V_O or other empty V_{Zn} to grow into vacancy clusters. During annealing, some hydrogen atoms might be released dynamically from V_{Zn} and leave mobile vacancies, which also contribute to the growth of vacancy clusters. During the above agglomeration process, more hydrogen impurities are also absorbed into the vacancy clusters, which occupy the space inside the vacancy clusters. These vacancy clusters containing hydrogen impurities are called hydrogen bubbles. Due to the occupation of hydrogen, the S parameter does not show an effective increase with the vacancy cluster growth.

With increasing annealing temperature, the hydrogen atoms will be released from the bubbles. Ip *et al.* have investigated in detail the thermal stability of hydrogen in ZnO. They found that annealing at 600–700 °C was enough to remove the implantation-incorporated hydrogen.[12] Therefore, the abrupt increase of the S parameter in the second period (600–700 °C) is apparently due to the release of hydrogen from the bubbles. As a result, a large number of microvoids are left. This leads to the large increase of the S parameter up to a maximum value of 1.17 at 700 °C.

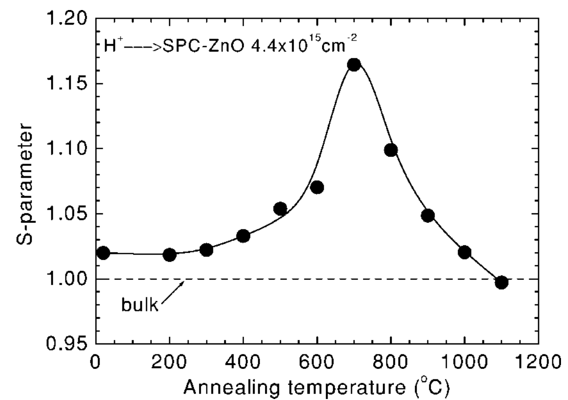

FIG. 4. S parameter in the central damaged region as a function of annealing temperature for the H^+-implanted ZnO.

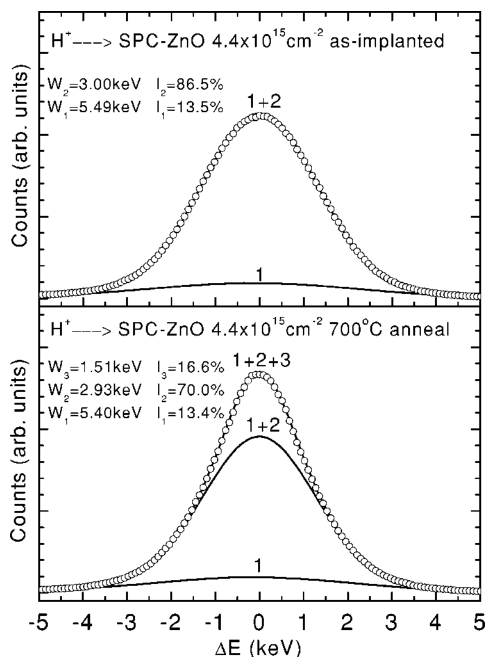

FIG. 5. Multi-Gaussian analysis of the summed Doppler broadening spectra (7–10 keV) measured for the H^+-implanted ZnO before and after annealing at 700 °C. The solid lines are from the fitting.

The large S parameter is generally supposed to be due to the formation of positronium, which is the bound state of a positron and electron, and which is usually formed in porous materials with large open spaces. To confirm this, we analyzed the Doppler broadening spectra in more detail. The summed spectra used above were analyzed by a multi-Gaussian fitting procedure[32,33] using the ACARFIT program.[34] Figure 5 shows the Doppler broadening spectra for the H^+-implanted ZnO before and after annealing at 700 °C. For the as-implanted sample, the spectrum can be fitted using two Gaussian components. The full widths at half-maximum (FWHMs) are 3.0 and 5.5 keV, which correspond to the low-momentum valence electrons and high-momentum core electrons, respectively. However, after annealing at 700 °C, a third component appears with a FWHM of only 1.51 keV, which is very close to the energy resolution of the detector (~1.3 keV). The intensity of this peak is 16.6%. Besides this narrow component, the width of the other two broad peaks are the same as that of the as-implanted sample, with only a variation in their respective intensities. The narrow peak is therefore attributable to the self-annihilation of the para-positronium (p-Ps), as it has nearly zero momentum.

To check the reliability of the above analysis, we measured a series of polymer samples using both beam-based Doppler broadening and conventional positron lifetime measurements. These polymers are: high-density polyethylene, polypropylene, polystyrene (PS), polycarbonate, and polytetrafluoroethylene. Besides these polymers, we also measured a Si single crystal and an amorphous SiO_2. The p-Ps intensity obtained from both lifetime [1/3 of ortho-positronium (o-Ps) intensity] and Doppler broadening measurements, and the width of the p-Ps component versus o-Ps lifetime are

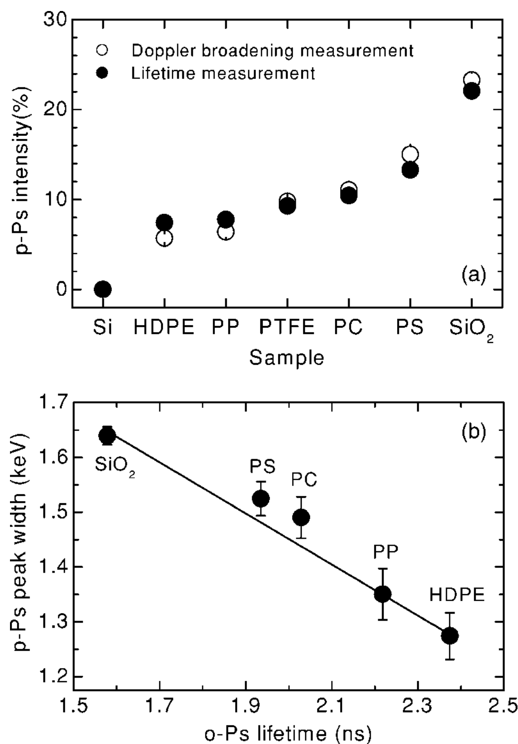

FIG. 6. (a) p-Ps intensity in a series of polymers together with a Si single crystal and an amorphous SiO_2 obtained by both Doppler broadening and positron lifetime measurements. (b) Width of the p-Ps component vs o-Ps lifetime.

shown in Fig. 6. It is seen that the p-Ps intensity obtained from Doppler broadening measurement shows very good agreement with that obtained by positron lifetime measurement. The width of the p-Ps component also shows a monotonic decrease with increasing o-Ps lifetime because of the confinement of p-Ps inside the free volume.[35] By comparison with these results, the diameter of the microvoids in H^+-implanted ZnO is then estimated to be close to that of the free volume in PS, which is in the subnanometer range.

We plotted the p-Ps intensity as a function of annealing temperature for the H^+-implanted ZnO in Fig. 7. The p-Ps

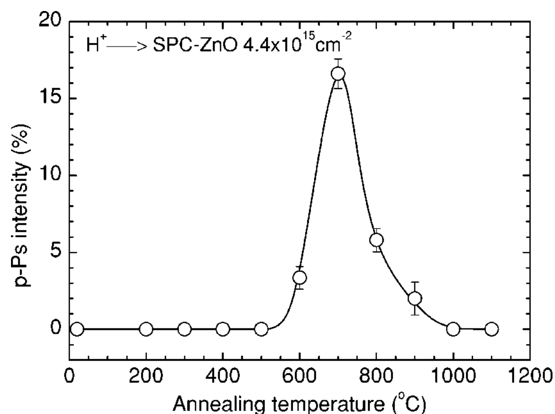

FIG. 7. p-Ps intensity obtained from the multi-Gaussian fitting for the H^+-implanted ZnO as a function of annealing temperature.

formation appears after annealing at 600 °C, and rapidly attains a maximum at 700 °C. As the p-Ps intensity is related to the number of microvoids or porosity, this indicates that hydrogen effusion from the bubble starts from 600 °C, and at 700 °C all the hydrogen atoms have been removed out of the bubbles. This result is in good agreement with that measured by Ip *et al.*[12]

The observation of p-Ps means that o-Ps should also be formed. From Fig. 2, we can see that positron lifetime shows a considerable increase after 700 °C annealing. There are two lifetime components: $\tau_1=173\pm6$ ps and $\tau_2=416\pm9$ ps. However, it is difficult to say that the second lifetime is due to the o-Ps annihilation because it is shorter than 500 ps, which is generally regarded as the criterion for positronium formation. This might be due to the spin conversion of Ps by paramagnetic impurities, which reduce o-Ps lifetime to a large extent. At a very high conversion rate, the o-Ps lifetime may be reduced to well below 500 ps.[36] On the other hand, in case of strong spin conversion of positronium, the ratio of o-Ps intensity to p-Ps intensity should be reduced to much smaller than 3:1. However, in our measurement, the ratio of the second lifetime component to the p-Ps component is 52:16.6, which is around or even a little higher than 3:1. This indicates that the second lifetime is not merely from o-Ps annihilation. In other words, it is a mixture of two components: one is the reduced o-Ps lifetime by spin conversion, which might be higher than the present value of 416 ps. Another is the positron lifetime annihilated at these microvoids without Ps formation. These two components may be too close to each other to be well separated.

As we cannot confirm the direct evidence of o-Ps from the positron lifetime measurements, the formation of positronium still needs to be verified by further investigations. In any case, the large increase of S parameter reveals the formation of subnanometer-sized microvoids in H^+-implanted ZnO, which might evolve from the hydrogen bubbles formed after annealing. It is a well-known phenomenon that hydrogen or helium will lead to bubble formation in metals as well as semiconductors.[37–39] They can be observed by transmission electron microscopy (TEM) if the implantation dose is high enough to form large bubbles (for example, in the He^+-implanted silicon with dose $>10^{16}$ cm^{-2}).[39] For low dose implantation, the bubble is too small to be recognized by TEM. However, the positron can detect small open volume defects down to the atomic scale; therefore, it is a unique tool for the study of small bubbles.

After further annealing at above 700 °C (the third period), S parameters begin to decrease. The p-Ps intensity, as shown in Fig. 7, also decreases. This might be due to the recovery of the microvoids. After the decrease of p-Ps intensity to zero at 1000 °C, which indicates full recovery of the microvoids, the S parameter is still a little higher than the bulk value. This might be due to the detection limit of microvoids by p-Ps, or to the existence of remaining small vacancies, which are removed after annealing at 1100 °C, as shown in Fig. 4.

B. Raman scattering characterization

Raman spectra were measured for the H^+-implanted sample after annealing at some selected temperatures. The

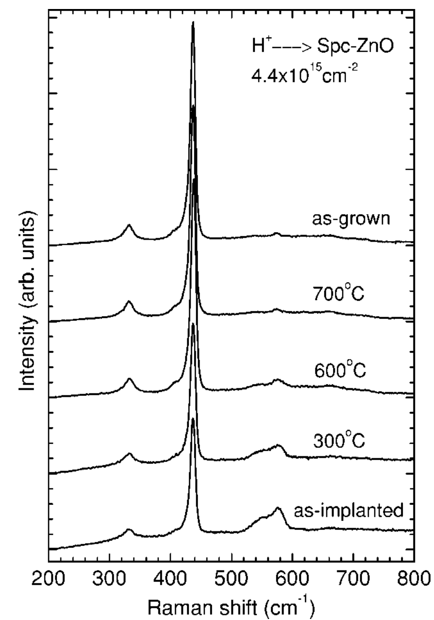

FIG. 8. Raman spectra measured for the H^+-implanted ZnO after annealing at different temperatures.

result is shown in Fig. 8. As ZnO has wurtzite structure, the expected phonon modes from group theory are[40] $A_1+2E_2+E_1$, where A_1 and E_1 are polar and split into TO and LO phonons with different frequencies. According to the phonon dispersion curve of ZnO, Raman spectra usually give the following phonon modes:[40,41] E_1 (LO) at 583 cm^{-1}, A_1 (LO) at 574 cm^{-1}, E_2 (high) at 437 cm^{-1}, E_1 (TO) at 408 cm^{-1}, A_1 (TO) at 381 cm^{-1}, and E_2 (low) at 101 cm^{-1}.

As seen in Fig. 8, for the as-grown ZnO, there is a predominant peak at about 437 cm^{-1} in the measured wave number range of 200–800 cm^{-1}, which is the high-frequency E_2 mode characteristic of the wurtzite structure. Besides this, there are also two weak peaks at 331 and 575 cm^{-1}. The peak at 331 cm^{-1} is due to the second-order phonon; i.e., $2E_2$(M). The smallest peak at 575 cm^{-1} corresponds to A_1 (LO), or a defect-induced mode. The other phonon modes are not seen in our measurements because of the backscattering geometry used in the experiment.

After H^+ implantation, the intensity of the peak at 331 cm^{-1} shows no change, but the peak at 575 cm^{-1} becomes stronger, and it also becomes much broader, extending from 520 to 600 cm^{-1}. As a result, the E_2 intensity decreases. The broad peak at 575 cm^{-1} is obviously not related to the hydrogen impurity, as we observed the same peak in other ion-implanted and even electron-irradiated samples. It is not related to the LO phonon either. The LO phonon band becomes stronger only in the sample with higher crystallinity. After ion implantation, it should decrease due to damage. This is contrary to our results. Therefore, we would rather believe that this broad peak is due to the implantation-induced defects.[42] Defect-induced modes are usually forbidden, but in defective crystals they appear because the Raman selection rules are relaxed. Implantation produces large amounts of defects, which cut the long-range lattice ordering. In this case, phonon frequencies close to the Γ point participate in the Raman spectrum. These contribu-

tions become larger when the phonon density of states (DOS) is high; i.e., when the phonon dispersion curve is relatively flat. Thus, a broad peak will appear in the Raman spectrum.

A close examination of the broad peak reveals also a low-frequency shoulder near 540 cm^{-1}. This is the two-phonon scattering of the LA phonon branch at 541 cm^{-1},[41] which is also relatively strong in defective crystals, because the two-phonon DOS is high. In any case, the broad peak at around 575 cm^{-1} is induced by the implantation damage, which is one of the very outstanding characteristics of ZnO phonon Raman spectra.

After annealing the implanted sample at 300 °C, the intensity of the broad peak is reduced. Further annealing at 600 °C causes a decrease to much smaller intensity. At 700 °C, it attains the same level as that of the as-grown sample, and the E_2 peak also shows full recovery. Many researchers have interpreted this broad vibration mode to be due to V_O or Zn interstitials (Zn_i),[43–45] as they found the enhancement of this peak in the oxygen-deficient condition. However, the interstitials in ZnO have much weaker thermal stability than vacancy defects, which has been verified by Gorelkinskii *et al.*[46] They found that the electron irradiation-induced interstitials in ZnO became mobile at 110 K, and were annealed out below room temperature. Therefore, only V_O might be the most probable candidate for the broad Raman peak at around 575 cm^{-1}.

The annealing results indicate that oxygen vacancies are removed at around 600–700 °C. They may disappear in two ways: one is the recombination with oxygen interstitials or migration into sinks; another way is the incorporation into hydrogen bubbles. The latter case is more probable, as its annealing process coincides completely with the bubble formation shown by the positron annihilation results

C. Cathodoluminescence measurements

The cathodoluminescence spectra for the H-implanted sample are presented in Fig. 9. For the as-grown sample, there is a predominant band-edge UV emission and a very weak visible emission, which can be attributed to free exciton and deep level defect recombination, respectively.[7] After H^+ implantation, both of the emissions are greatly reduced. This is due to the introduction of defects by implantation. Some of the defects act as nonradiative recombination centers and therefore compete with the UV and visible emission. After 300 °C annealing, the UV emission recovers, and becomes even stronger than that in the as-grown sample. This means that most of the nonradiative recombination centers are removed. The enhancement of UV emission compared with the as-grown sample indicates that nonradiative recombination centers may also exist in the as-grown sample. However, after disappearance of the nonradiative recombination process by annealing at 300 °C, the deep level emission is still very weak. Further annealing at 600 °C causes nearly no change of the spectra. Only after annealing at 700 °C, the deep level emission begins to increase and, consequently, the UV emission is weakened.

Previous studies showed that in the hydrogen plasma-treated ZnO, the deep level defects were passivated by hydrogen, which led to the strong UV emission.[7–9] It is therefore reasonable to assume that in our H^+-implanted ZnO, the suppression of deep level emission between 300 and 600 °C is also due to the passivation of those defect centers by hydrogen. This is further confirmed by a sudden increase of deep level emission after annealing at 700 °C, which causes the release of the hydrogen. The origin of the defect responsible for this deep level emission is still under debate.[47–51] Thus, we cannot specify this defect center. Further detailed research work is needed.

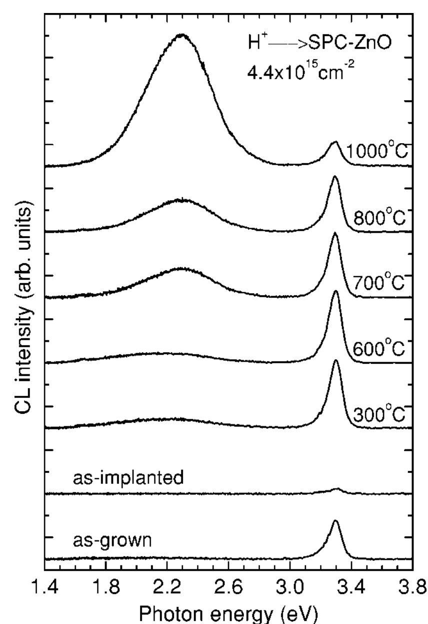

FIG. 9. Cathodoluminescence spectra measured for the H^+-implanted ZnO after annealing at different temperatures.

Upon increasing temperature up to 1000 °C, the visible emission shows a considerable increase, indicating that more deep level defects are introduced. A similar phenomenon was also observed in the as-grown ZnO after high-temperature annealing.[21] This might be due to the defect formation at high temperatures. Nevertheless, the positron annihilation results show a gradual decrease of the S parameter after annealing above 700 °C. This means that the defects observed by positrons are not responsible for the deep level emission. The hydrogen atoms not only interact with vacancy defects, but also passivate other defects, such as O_i and O_{Zn}, which were suggested to be responsible for the deep level emission.[49,50] These hydrogen atoms may have the same thermal stability as those in the vacancies; therefore, they suppress the deep level emission below 700 °C.

IV. CONCLUSION

Zinc vacancies are produced by H^+ implantation in ZnO. They are filled with hydrogen impurities. After annealing, hydrogen bubbles are formed due to the coalescence of the small vacancies. With further annealing at around 700 °C, all the hydrogen impurities are released from these bubbles and leave empty microvoids. These microvoids are recovered at about 1000 °C. Raman-scattering measurements show

production of oxygen vacancies after implantation, and they disappear at around 600–700 °C accompanying the formation of hydrogen bubbles. The implanted hydrogen ions passivate deep level defects before their release, resulting in the enhancement of UV emission.

ACKNOWLEDGMENTS

The authors would like to thank Professor Hiroshi Harima for the very fruitful discussions of the Raman scattering data.

*Electronic address: chenzq@taka.jaeri.go.jp

[1] P. Zu, Z. K. Tang, G. K. L. Wong, M. Kawasaki, A. Ohtomo, K. Koinuma, and Y. Segawa, Solid State Commun. **103**, 459 (1997).
[2] D. M. Bagnall, Y. F. Chen, Z. Zhu, T. Yao, S. Koyama, M. Y. Sen, and T. Goto, Appl. Phys. Lett. **70**, 2230 (1997).
[3] C. G. Van de Walle, Phys. Rev. Lett. **85**, 1012 (2000).
[4] S. F. J. Cox *et al.*, Phys. Rev. Lett. **86**, 2601 (2001).
[5] D. M. Hofmann, A. Hofstaetter, F. Leiter, H. Zhou, F. Henecker, B. K. Meyer, S. B. Orlinskii, J. Schmidt, and P. G. Baranov, Phys. Rev. Lett. **88**, 045504 (2002).
[6] N. H. Nickel and K. Fleischer, Phys. Rev. Lett. **90**, 197402 (2003).
[7] T. Sekiguchi, N. Ohashi, and Y. Terada, Jpn. J. Appl. Phys., Part 2 **36**, L289 (1997).
[8] N. Ohashi, T. Ishigaki, N. Okada, T. Sekiguchi, I. Sakaguchi, and H. Haneda, Appl. Phys. Lett. **80**, 2869 (2002).
[9] N. Ohashi, T. Ishigaki, N. Okada, H. Taguchi, I. Sakaguchi, S. Hishita, T. Sekiguchi, and H. Haneda, J. Appl. Phys. **93**, 6386 (2003).
[10] A. Y. Polyakov, N. B. Smirnov, A. V. Govorkov, K. Ip, M. E. Overberg, Y. W. Heo, D. P. Norton, S. J. Pearton, B. Luo, F. Ren, and J. M. Zavada, J. Appl. Phys. **94**, 400 (2003).
[11] E. V. Lavrov, J. Weber, F. Borrnert, Chris G. Van de Walle, and R. Helbig, Phys. Rev. B **66**, 165205 (2002).
[12] K. Ip, M. E. Overberg, Y. W. Heo, D. P. Norton, S. J. Pearton, C. E. Stutz, B. Luo, F. Ren, D. C. Look, and J. M. Zavada, Appl. Phys. Lett. **82**, 385 (2003).
[13] M. D. McCluskey, S. J. Jokela, K. K. Zhuravlev, P. J. Simpson, and K. G. Lynn, Appl. Phys. Lett. **81**, 3807 (2002).
[14] K. Ip, M. E. Overberg, Y. W. Heo, D. P. Norton, S. J. Pearton, S. O. Kucheyev, C. Jagadish, J. S. Williams, R. G. Wilson, and J. M. Zavada, Appl. Phys. Lett. **81**, 3996 (2002).
[15] A. Y. Polyakov *et al.*, J. Appl. Phys. **94**, 2895 (2003).
[16] F. D. Auret, S. A. Goodman, M. Hayes, M. J. Legodi, H. A. van Laarhoven, and D. C. Look, J. Phys.: Condens. Matter **13**, 8989 (2001).
[17] R. Krause-Rehberg and H. S. Leipner, *Positron Annihilation in Semiconductors, Defect Studies*, in Springer Series in Solid-State Sciences Vol. 127 (Springer, Berlin, 1999).
[18] R. M. de la Cruz, R. Pareja, R. González, L. A. Boatler, and Y. Chen, Phys. Rev. B **45**, 6581 (1992).
[19] S. Brunner, W. Puff, A. G. Balogh, and P. Mascher, Mater. Sci. Forum **363–365**, 141 (2001).
[20] A. Uedono, T. Koida, A. Tsukazaki, M. Kawasaki, Z. Q. Chen, SF. Chichibu, and H. Koinuma, J. Appl. Phys. **93**, 2481 (2003).
[21] Z. Q. Chen, S. Yamamoto, M. Maekawa, A. Kawasuso, X. L. Yuan, and T. Sekiguchi, J. Appl. Phys. **94**, 4807 (2003).
[22] F. Tuomisto, V. Ranki, K. Saarinen, and D. C. Look, Phys. Rev. Lett. **91**, 205502 (2003).
[23] Z. Q. Chen, M. Maekawa, S. Yamamoto, A. Kawasuso, X. L. Yuan, T. Sekiguchi, R. Suzuki, and T. Ohdaira, Phys. Rev. B **69**, 035210 (2004).
[24] R. Suzuki, Y. Kobayashi, T. Mikado, H. Ohgaki, M. Chiwaki, T. Yamazaki, and T. Tomimasu, Jpn. J. Appl. Phys., Part 2 **30**, L532 (1991).
[25] T. Sekiguchi and K. Sumino, Rev. Sci. Instrum. **66**, 4277 (1995).
[26] J. P. Biersack and L. G. Haggmark, Nucl. Instrum. Methods **174**, 257 (1980).
[27] S. M. Myers, M. I. Baskes, H. K. Birnbaum, J. W. Corbett, G. G. DeLeo, S. K. Estreicher, E. E. Haller, P. Jena, N. M. Johnson, R. Kirchheim, S. J. Pearton, and M. J. Stavola, Rev. Mod. Phys. **64**, 559 (1992).
[28] H. Ohkubo, S. Sugiyama, K. Fukuzato, M. Takenaka, N. Tsukuda, and E. Kuramoto, J. Nucl. Mater. **283–287**, 858 (2000).
[29] P. Asoka-Kumar, H. J. Stein, and K. G. Lynn, Appl. Phys. Lett. **64**, 1684 (1994).
[30] M. Fujinami, R. Suzuki, T. Ohdaira, and T. Mikado, Phys. Rev. B **58**, 12 559 (1998).
[31] A. Uedono *et al.*, J. Appl. Phys. **93**, 3228 (2003).
[32] G. Dlubek, H. M. Fretwell, and M. A. Alam, Macromolecules **33**, 187 (2000).
[33] A. Alba Garcia, L. D. A. Siebbeles, A. Rivera, H. Schut, S. W. H. Eijt, R. Escobar Galindo, and A. van Veen, Mater. Sci. Forum **363–365**, 287 (2001).
[34] P. Kirkegaard, N. J. Pederson, and M. Eldrup, Risø National Laboratory, DK-4000 Roskilde, Denmark, 1989.
[35] H. Nakanishi and Y. C. Jean, in *Positron and Positronium Chemistry*, edited by D. M. Schrader and Y. C. Jean (Elsevier Science, Amsterdam, 1988) p. 159.
[36] S. Dannefaer, T. Friessnegg, D. Kerr, A. Uedono, X. Li, and S. Tanigawa, Phys. Rev. B **54**, 15 051 (1996).
[37] J. B. Condon and T. Schober, J. Nucl. Mater. **207**, 1 (1993).
[38] G. F. Cerofolini, F. Corni, S. Frabboni, C. Nobili, G. Ottaviani, and R. Tonini, Mater. Sci. Eng., R. **27**, 1 (2000).
[39] V. Raineri, M. Saggio, and E. Rimini, J. Mater. Res. **15**, 1449 (2000).
[40] T. C. Damen, S. P. S. Porto, and B. Tell, Phys. Rev. **142**, 570 (1966).
[41] J. M. Calleja and M. Cardona, Phys. Rev. B **16**, 3753 (1977).
[42] F. Reuss, C. Kirchner, Th. Gruber, R. Kling, S. Maschek, W. Limmer, A. Waag, and P. Ziemann, J. Appl. Phys. **95**, 3385 (2004).
[43] J. N. Zeng, J. K. Low, Z. M. Ren, T. Liew, and Y. F. Lu, Appl. Surf. Sci. **197**, 362 (2002).
[44] S.-H. Jeong, J.-K. Kim, and B.-T. Lee, J. Phys. D **36**, 2017 (2003).
[45] C. J. Youn, T. S. Jeong, M. S. Han, and J. H. Kim, J. Cryst. Growth **261**, 526 (2004).

[46] Yu. V. Gorelkinskii and G. D. Watkins, Phys. Rev. B **69**, 115212 (2004).
[47] K. Vanheusden, C. H. Seager, W. L. Warren, D. R. Tallant, and J. A. Voigt, Appl. Phys. Lett. **68**, 403 (1996).
[48] D. C. Reynolds, D. C. Look, B. Jogai, J. E. Van Nostrand, R. Jones, and J. Jenny, Solid State Commun. **106**, 701 (1998).
[49] M. Liu, A. H. Kitai, and P. Mascher, J. Lumin. **54**, 35 (1992).
[50] B. Lin, Z. Fu, and Y. Jia, Appl. Phys. Lett. **79**, 943 (2001).
[51] N. Y. Garces, L. Wang, L. Bai, N. C. Giles, L. E. Halliburton, and G. Cantwell, Appl. Phys. Lett. **81**, 622 (2002).